Solid Phase Epitaxy of Rutile-type GeO_2 on TiO_2 (001)

Yo Nagashima,[1] Shohei Osawa,[2] Daichi Oka,[2] and Yasushi Hirose[2*]

1. Department of Chemistry, School of Science, The University of Tokyo, 7-3-1 Hongo, Bunkyo, Tokyo 113-0033, Japan
2. Department of Chemistry, Graduate School of Science, Tokyo Metropolitan University, 1-1 Minami-Osawa, Hachioji, Tokyo 192-0397, Japan

* Author to whom correspondence should be addressed: hirose@tmu.ac.jp

Abstract

Rutile-type GeO_2 (r-GeO_2) is an ultra-wide bandgap oxide semiconductor, which attracts growing interest because of its ambipolar dopability and high carrier mobility predicted by recent first principles calculations. While epitaxial thin films of r-GeO_2 have been synthesized using various vapor phase epitaxy techniques, desorption of germanium suboxide limits the growth conditions in a narrow range. Here, we demonstrated solid phase epitaxy (SPE) of r-GeO_2 thin films on TiO_2 (001) substrates. Amorphous GeO_2 thin films fabricated using pulsed laser deposition at ≤ 250 °C were crystallized by post-deposition annealing at 700 °C. X-ray diffraction and cross-sectional scanning transmission electron microscopy analysis revealed that the amorphous GeO_2 thin films epitaxially crystallized to r-GeO_2 phase without any impurity phases. The epitaxial cyrstallization of r-GeO_2 was significantly promoted by introducing a seed layer of a rutile $Ge_xSn_{1-x}O_2$ epitaxial thin film, which coherently grown on the TiO_2 substrate, probably due to chemical interactions between the amorphous film and the seed layer. The crystallinity of the SPE-grown r-GeO_2 was comparable to that synthesized via vapor phase epitaxy, indicating that the SPE is an alternative route for synthesizing r-GeO_2 epitaxial thin films.

Ultra-wide bandgap semiconductors, of which bandgap (E_g) is larger than conventional wide bandgap semiconductors such as GaN and SiC, have been extensively studied for power electronics and ultraviolet optoelectronics applications owing to their high electric breakdown field and bandgap energy corresponding to ultraviolet light.[1-3] Among ultra-wide bandgap semiconductors, rutile-type GeO_2 (r-GeO_2) (E_g~4.7 eV)[4] attracts growing interest because of its advantageous features for power electronics applications, such as ambipolar dopability and high carrier mobility, which are predicted by first-principles calculations,[5–8] as well as high thermal conductivity.[9]

To experimentally validate these unique properties expected for r-GeO_2 and to fabricate a device structure, synthesis of r-GeO_2 in both bulk single crystal and epitaxial thin film forms is indispensable. Bulk single crystals of r-GeO_2 have been synthesized since the 1960s by chemical vapor transport and solution processes.[6,10-13] Recently, n-type dopability with high carrier electron concentration of up to 2.2×10^{20} cm^{-3} was reported for Sb-doped r-GeO_2 bulk single crystals synthesized via top seeded solution growth.[13] On the other hand, there is no report on successful doping in r-GeO_2 epitaxial thin films, although various vapor phase deposition techniques such as molecular beam epitaxy (MBE),[14] pulsed laser deposition (PLD),[15,16] mist chemical vapor deposition,[17,18] metal-organic chemical vapor deposition,[19] and low-pressure chemical vapor deposition[20] have been proposed after the first demonstration using MBE.[14]

There are two main difficulties in synthesizing r-GeO_2 thin films. The first one is thermodynamic stability competing against the α-quartz phase and the amorphous phase, of which formation energies are comparable to that of r-GeO_2 phase.[6,14] The second one is the desorption of germanium suboxide (GeO),[21–23] which limits the growth parameters (e.g. growth temperature and partial oxygen pressure during the deposition) in a narrow range.[14] As a result, thin films of r-GeO_2 frequently suffered from the coexistence of the other phases and/or poorly crystallized regions.[15,24,25]

In this study, we demonstrated solid phase epitaxy (SPE) of r-GeO_2 thin films on TiO_2

(001) substrates as an alternative route for synthesizing r-GeO_2 epitaxial thin films. In the SPE process, amorphous GeO_2 films were crystallized epitaxially from the film/substrate interface by post-deposition annealing. In the previous studies on the crystallization of amorphous GeO_2 into r-GeO_2, the synthesized films were polycrystalline,[26,27] some of which are mixed phase with α-quartz phase or Ge. It was revealed that the SPE of the r-GeO_2 was significantly enhanced by introducing an epitaxial rutile $Ge_xSn_{1-x}O_2$ (GSO) film as a seed layer, on which epitaxial crystallization of r-GeO_2 was promoted probably due to chemical interactions between the amorphous film and the seed layer.

The SPE of r-GeO_2 was conducted by the following three steps: (Step 1) A ~10-15 nm-thick (001)-oriented rutile $Ge_xSn_{1-x}O_2$ (GSO) thin film (seed layer) was epitaxially grown on a rutile TiO_2 (001) substrate to promote the epitaxial crystallization as discussed later. (Step 2) An amorphous GeO_2 film was deposited on the GSO seed layer at low temperature. (Step 3) The amorphous GeO_2 film was crystallized by annealing inside the growth chamber without exposure to air to avoid degradation of the amorphous by humidity.

The GSO seed layer (Ge content x~0.4) and the amorphous GeO_2 film were fabricated by PLD. The growth condition of the GSO seed layer was described elsewhere.[18] The amorphous GeO_2 thin films were deposited at substrate temperature of 250 °C by ablating a ceramic pellet of GeO_2 using a KrF excimer laser (Coherent, COMPex pro 102). The pulse repetition rate and the laser fluence were set at 2 Hz and 1-2 $J \cdot cm^{-2} \cdot pulse^{-1}$, respectively, to control the deposition rate at ~100 nm/h. The base pressure in the growth chamber was lower than 1×10^{-7} Torr. Partial O_2 pressure was kept at 1×10^{-4} Torr during the deposition of amorphous GeO_2 thin films and the post-annealing for crystallization, where the supplied O_2 gas was activated into radicals by an electron cyclotron resonance plasma source (Tectra, Gen2). It is noted that GeO_2 film deposited at substrate temperature of 600 °C was totally evaporated during the deposition (Supplemental Fig. S1).

Crystal structure and density of the GeO_2 thin films were evaluated by X-ray diffraction (XRD) and X-ray reflection (XRR) measurements, respectively, using a four-circle diffractometer (Bruker AXS, D8 DISCOVER). The structure of the amorphous GeO_2 thin film was evaluated by Raman spectroscopy (Renishaw, inVia Qontor). The microscopic structures and the chemical composition distribution in the r-GeO_2 thin film were investigated by cross-sectional scanning transmission electron microscopy (STEM) (JEOL, JEM-ARM200F-B, 200 kV) with a detector for energy dispersive X-ray spectroscopy (EDS) (Thermo Fisher Scientific, NSS). The specimen for STEM observation was prepared by using a focused ion beam system (Hitachi High-Tech, NB5000). The surface morphologies of the films were observed by atomic force microscopy (AFM) (SII-nanotechnology, SPI4000 with SPA400). Thicknesses of the thin films were examined by XRR measurement or using a stylus surface profiler (Kosaka Laboratory Ltd., Surfcorder ET200 A).

Figure 1a shows θ-2θ XRD patterns of the GeO_2 thin films deposited at 250 °C on the GSO seed layer and annealed at various temperature. It is noted that the GeO_2 film deposited at 600 °C was totally evaporated during the deposition (Supplemental Fig. S1). The GeO_2 thin film annealed at 600 °C showed diffraction peaks only from the GSO seed layer and the TiO_2 substrate, indicating that the GeO_2 film was amorphous. On the other hand, a clear 002 diffraction peak of r-GeO_2 was observed for the film annealed at 700 and 750 °C without the diffraction peaks from the α-quartz type GeO_2 nor the r-GeO_2 with different crystallographic orientations. XRD reciprocal space map (RSM) of the r-GeO_2 films around the 112 diffraction (Fig. 1b) and phi scan measurement (Fig. 1c) verified the epitaxial growth of (001)-oriented r-GeO_2 without any rotational domains. Epitaxial growth of the r-GeO_2 was also confirmed at partial O_2 pressure of 1×10^{-3} Torr without the plasma activation (Supplemental Fig. S2). The GeO_2 film annealed at 800 °C showed diffraction peaks only from the substrates (Fig. 1a) indicating the evaporation of the r-GeO_2 film and the GSO seed layer during the annealing. Partial evaporation of GeO_2 layer

was also suggested in the films annealed at 700 and 750 °C (Supplemental Table S3). Based on these results, controlling the temperature of the post deposition annealing at 700-750 °C is required for the SPE of r-GeO_2. Although this temperature range is not wider than that of vapor phase epitaxy, the high temperature limit could be extended by suppressing the evaporation of GeO_2 under more oxidative conditions as reported in the previous studies on the crystallization of amorphous GeO_2 thin films.[26,27] It is also speculated that slightly introducing O vacancies in the amorphous GeO_2 thin film, which kinetically enhances atomic diffusion, enables the crystallization at lower temperature than 700 °C:[28] Off-stoichiometry of the amorphous GeO_2 thin film was not observed by Raman spectroscopy (Supplemental Figure S4).

The lattice constants of the r-GeO_2 epitaxial thin films determined from the RSM (a = 4.410 Å, c = 2.859 Å) were close to those reported for bulk r-GeO_2 (a = 4.3975 Å, c = 2.8625 Å)[29], indicating that the r-GeO_2 film was almost relaxed. The full width of half maximum (FWHM) of the rocking curve of 002 diffraction was 0.365° (Fig. 1d), which is comparable to the values reported for the r-GeO_2 epitaxial thin films synthesized from vapor phase using PLD.[15,16]

For the SPE of r-GeO_2 on TiO_2, introducing the GSO seed layer is crucial. Most of the amorphous films deposited directly on the TiO_2 (001) substrate did not crystallize by the annealing at 700 °C. Even in the case of epitaxially crystallized film (Fig. 1a), the crystallinity of the film was lower than those grown on the GSO seed layer: FWHM of the rocking curve of 002 diffraction increased from 0.365° to 1.03° (Fig. 1d). Notably, the GSO seed layer coherently grew on the TiO_2 substrate without strain relaxation (a = 4.594 Å, c = 3.088 Å) as shown in the RSM (Fig. 1b), meaning that lattice mismatch between the r-GeO_2 thin film and the TiO_2 substrate (a = 4.594 Å, c = 2.959Å) was not reduced by the insertion of the GSO layer. This is in stark contrast to the previous reports on the epitaxial growth of r-GeO_2,[14,18] where the introduction of a GSO buffer layer stabilizes rutile structure through the reduction of the lattice mismatch between the r-GeO_2 thin film and the substrate. This result suggested that the epitaxial nucleation of the r-GeO_2 at the film/substrate interface was dominated not only by the elastic energy originating from the

lattice mismatch but also by the chemical interactions between the film and the substrate.

The microscopic structure of the r-GeO_2 thin film was further investigated by cross-sectional STEM observation. Fig. 2a shows the cross-sectional high-angular annular dark field (HAADF) images of the r-GeO_2 epitaxial thin film grown on the GSO seed layer. Selected area electron diffraction patterns (Figs. 2b, c) show diffraction spots only from the (001)-oriented r-GeO_2, confirming the epitaxial crystallization of r-GeO_2. *Z*-contrast in the HAADF-STEM image and the results of EDS mapping (Fig. 3) show a sharp and flat interface between the r-GeO_2 thin film and the GSO seed layer verifying that no interdiffusion occurred at the interface during the SPE process. The HAADF-STEM images of the r-GeO_2 film show almost no spatial inhomogeneity in its contrast except for the small regions probably corresponding to dislocations and grain boundaries. Considering the large difference in atomic density between the amorphous and r-GeO_2, the amorphous GeO_2 film was fully crystallized into the rutile phase from the film/seed layer interface to the film surface.

The θ-2θ peak and the rocking curve of the GSO seed layer became broader after the post deposition annealing (Supplemental Figure S5), which indicates degradation of crystallinity during the annealing. Based on the results of STEM-EDS mapping (Fig. 3), this degradation did not originate from the interdiffusion between the GSO and the GeO_2, which was also supported by a negligible shift in the XRD θ-2θ peak of the seed layer after the annealing (Fig. S2). Because the GSO seed layer annealed without the amorphous GeO_2 layer also showed a broadening of the XRD peaks (Fig. S2), we speculate that the deterioration of the seed layer was caused by the thermal instability of GSO.[30]

Figure 4 shows AFM images of the amorphous GeO_2 and the SPE-grown r-GeO_2 thin films (thickness of ~120 nm). While the surface of the amorphous GeO_2 (Fig. 4a) was smooth (root-mean-square roughness r_{RMS} = 0.24 nm), grain-like morphology appeared after the crystallization (Fig. 4b). Surface roughness of the SPE-grown r-GeO_2 thin film (r_{RMS} = 3.94 nm) was larger than the amorphous GeO_2 (r_{RMS} = 0.24 nm), although the value was comparable to or

slightly better than the values reported for r-GeO_2 thin films grown by vapor phase epitaxy.[16,19,20] The increase of the roughness is, at least in part, due to the evaporation of GeO during the annealing (Supplemental Table S3), although it might also be attributable to the large difference in density between the amorphous GeO_2 thin films (~4.2 g cm^{-3}, slightly larger than bulk GeO_2 glass[31–33]) and the r-GeO_2 epitaxial thin films (~6.2 g cm^{-3}, almost the same as bulk r-GeO_2 of 6.27 g cm^{-3}).

In summary, (001)-oriented r-GeO_2 epitaxial thin films were grown on TiO_2 (001) substrates by the SPE of amorphous GeO_2 thin films deposited using PLD. The epitaxial crystallization of the amorphous GeO_2 film was significantly enhanced by the insertion of an epitaxial GSO seed layer. The crystallinity and surface roughness of the SPE-grown r-GeO_2 thin films were almost comparable to the r-GeO_2 epitaxial thin films synthesized by vapor phase epitaxy. These results demonstrate that the SPE is a useful technique with a potential for enlarging the process window of r-GeO_2, which will promote future studies on its physical properties and device applications.

Supplementary Material

See the supplementary Material for details on the XRD pattern of the GeO_2 deposited at 600 °C, XRD patterns of the r-GeO_2 thin films crystallized without the plasma activation of O_2 gas, thickness of the GeO_2 layer before and after crystallization, Raman spectrum of the amorphous GeO_2 layer, and XRD patterns of the GSO seed layer after the post deposition annealing.

This work was supported in part by project JPNP20004 subsidized by the New Energy and Industrial Technology Development Organization (NEDO), Tokyo Ohka Foundation for The Promotion of Science and Technology, and Advanced Research Infrastructure for Materials and Nanotechnology in Japan (ARIM) of the Ministry of Education, Culture, Sports, Science and Technology (MEXT) Proposal Number JPMXP1223NM0167. We thank Dr. Fumihiko Uesugi and Yoshiko Nakayama for the STEM analyses.

References

[1] J.Y. Tsao, S. Chowdhury, M.A. Hollis, D. Jena, N.M. Johnson, K.A. Jones, R.J. Kaplar, S. Rajan, C.G. Van de Walle, E. Bellotti, C.L. Chua, R. Collazo, M.E. Coltrin, J.A. Cooper, K.R. Evans, S. Graham, T.A. Grotjohn, E.R. Heller, M. Higashiwaki, M.S. Islam, P.W. Juodawlkis, M.A. Khan, A.D. Koehler, J.H. Leach, U.K. Mishra, R.J. Nemanich, R.C.N. Pilawa-Podgurski, J.B. Shealy, Z. Sitar, M.J. Tadjer, A.F. Witulski, M. Wraback, and J.A. Simmons, Adv. Electron. Mater. **4**, 1600501 (2018).

[2] M. Kneissl, T.-Y. Seong, J. Han, and H. Amano, Nat. Photonics **13**, 233 (2019).

[3] J.B. Varley, B. Shen, and M. Higashiwaki, J. Appl. Phys. **131**, 230401 (2022).

[4] M. Stapelbroek and B.D. Evans, Solid State Commun. **25**, 959 (1978).

[5] K. Bushick, K.A. Mengle, S. Chae, and E. Kioupakis, Appl. Phys. Lett. **117**, 182104 (2020).

[6] C.A. Niedermeier, K. Ide, T. Katase, H. Hosono, and T. Kamiya, J. Phys. Chem. C **124**, 25721 (2020).

[7] S. Chae, J. Lee, K.A. Mengle, J.T. Heron, and E. Kioupakis, Appl. Phys. Lett. **114**, 102104 (2019).

[8] K.A. Mengle, S. Chae, and E. Kioupakis, J. Appl. Phys. **126**, (2019).

[9] S. Chae, K.A. Mengle, R. Lu, A. Olvera, N. Sanders, J. Lee, P.F.P. Poudeu, J.T. Heron, and E. Kioupakis, Appl. Phys. Lett. **117**, 102106 (2020).

[10] V.G. Hill and L.L.Y. Chang, Am. Mineral. **53**, 1744 (1968).

[11] D.E. Swets, J. Cryst. Growth **8**, 311 (1971).

[12] S. Chae, L.A. Pressley, H. Paik, J. Gim, D. Werder, B.H. Goodge, L.F. Kourkoutis, R. Hovden, T.M. McQueen, E. Kioupakis, and J.T. Heron, J. Vac. Sci. Technol. A **40**, (2022).

[13] Z. Galazka, R. Blukis, A. Fiedler, S. Bin Anooz, J. Zhang, M. Albrecht, T. Remmele, T. Schulz, D. Klimm, M. Pietsch, A. Kwasniewski, A. Dittmar, S. Ganschow, U. Juda, K. Stolze, M. Suendermann, T. Schroeder, and M. Bickermann, Phys. Status Solidi (B) 2400326 (2024).

[14] S. Chae, H. Paik, N.M. Vu, E. Kioupakis, and J.T. Heron, Appl. Phys. Lett. **117**, 072105 (2020).

[15] G. Deng, K. Saito, T. Tanaka, M. Arita, and Q. Guo, Appl. Phys. Lett. **119**, 182101 (2021).

[16] G. Deng, Y. Huang, Z. Chen, K. Saito, T. Tanaka, M. Arita, and Q. Guo, Mater. Lett. **326**, 132945 (2022).

[17] H. Takane and K. Kaneko, Appl. Phys. Lett. **119**, 062104 (2021).

[18] K. Shimazoe, T. Ogawa, and H. Nishinaka, Appl. Phys. Express **17**, 105501 (2024).

[19] I. Rahaman, B.G. Duersch, H.D. Ellis, M.A. Scarpulla, and K. Fu, Appl. Phys. Lett. **125**, 102103 (2024).

[20] F. Golbasi, B. Liu, J. Hwang, and F. Akyol, J. Alloys Compd. **1014**, 178591 (2025).

[21] W. Chen, K. Egbo, J. Kler, A. Falkenstein, J. Lähnemann, and O. Bierwagen, APL Mater. **13**, 011107 (2025).

[22] W. Chen, K. Egbo, H. Tornatzky, M. Ramsteiner, M.R. Wagner, and O. Bierwagen, APL Mater. **11**, 071110 (2023).

[23] C.H. Lee, T. Tabata, T. Nishimura, K. Nagashio, K. Kita, and A. Toriumi, Appl. Phys. Express **2**, 071404 (2009).

[24] H. Takane and K. Kaneko, Appl. Phys. Lett. **120**, 099903 (2022).

[25] H. Takane, Y. Ota, T. Wakamatsu, T. Araki, K. Tanaka, and K. Kaneko, Phys. Rev. Mater. **6**, 084604 (2022).

[26] P.G. Nalam, D. Das, S. Tan, and C. V. Ramana, ACS Appl. Electron. Mater. **4**, 3115 (2022).

[27] A.M. Abed and R.L. Peterson, J. Vac. Sci. Technol. A **42**, 063403 (2024).

[28] S.K. Wang, K. Kita, T. Nishimura, K. Nagashio, and A. Toriumi, Jpn. J. Appl. Phys. **50**, 10PE04 (2011).

[29] W.H. Baur and A.A. Khan, Acta Crystallogr. Sect. B Struct. Crystallogr. Cryst. Chem. **27**, 2133 (1971).

[30] F. Liu, N.J. Szymanski, K. Noordhoek, H. Shin, D. Kim, C.J. Bartel, and B. Jalan, Nano Lett. **25**, 299 (2025).

[31] S. Petitgirard, G. Spiekermann, K. Glazyrin, J. Garrevoet, and M. Murakami, Phys. Rev. B **100**, 214104 (2019).

[32] M. Akaogi, T. Suzuki, R. Kojima, T. Honda, E. Ito, and I. Nakai, Geophys. Res. Lett. **25**, 3635 (1998).

[33] K. Kamiya, T. Yoko, Y. Itoh, and S. Sakka, J. Non. Cryst. Solids **79**, 285 (1986).

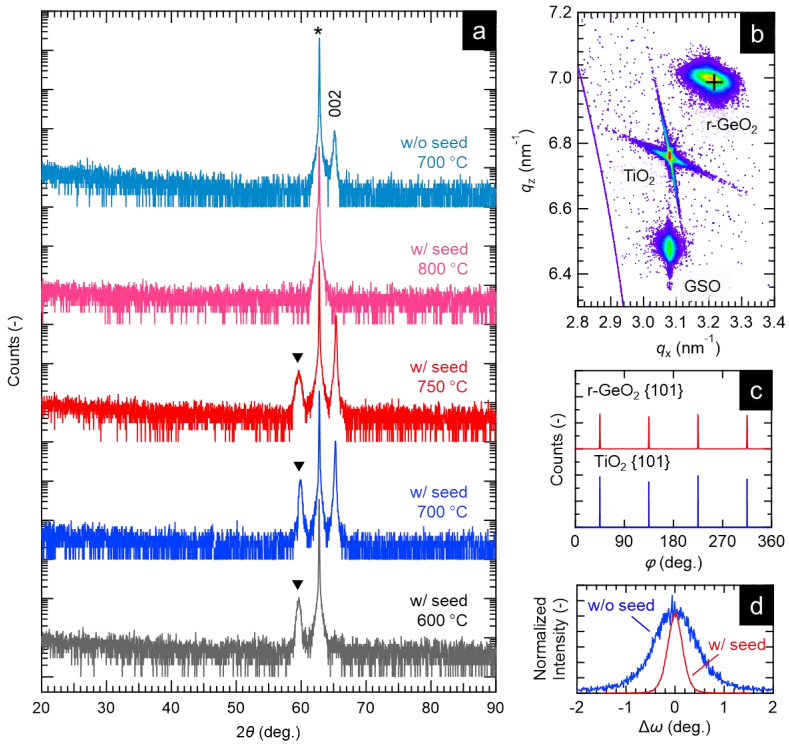

Figure 1. (a) θ-2θ XRD patterns of the GeO_2/GSO (001)/TiO_2 (001) (w/ seed) after the post deposition annealing at 600, 700, 750 and 800 °C. Diffraction pattern of the GeO_2/TiO_2 (001) (w/o seed) crystallized at 700 °C is also plotted for comparison. Asterisk and triangles denote the diffraction peaks of the TiO_2 substrate and the GSO seed layer, respectively. (b) RSM around 112 diffraction peak of the r-GeO_2 (001)/GSO (001)/TiO_2 (001) crystallized at 700 °C. Cross indicates the peak position calculated from the lattice constants of bulk r-GeO_2. (c) Phi-scan of the 101 diffraction for the r-GeO_2 (001)/GSO (001)/TiO_2 (001). (d) Rocking curves of 002 diffraction for r-GeO_2 (001) epitaxial thin films crystallized at 700 °C with and without the GSO seed layer.

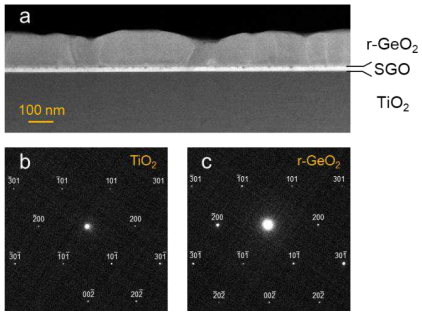

Figure 2. (a) Cross-sectional HAADF STEM image and (b, c) SAED patterns of the r-GeO_2 (001)/GSO (001)/TiO_2 (001) synthesized by the SPE process. Diffraction pattern (b) and (c) were obtained for the TiO_2 substrate and the r-GeO_2 film, respectively along the [010] zone axis.

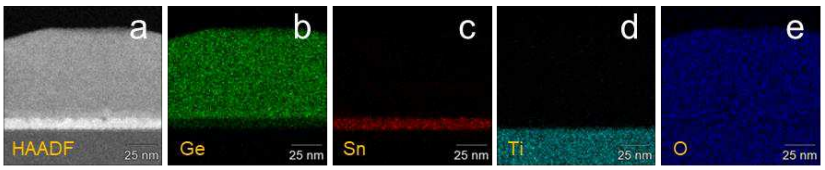

Figure 3. (a) STEM-HAADF image of the EDS mapping area of the r-GeO_2 (001)/GSO (001)/TiO_2 (001). (b-e) Elemental maps constructed from the EDS signals of (b) Ge K-line, (c) Sn L-line, (d) Ti K-line, and (e) O K-line.

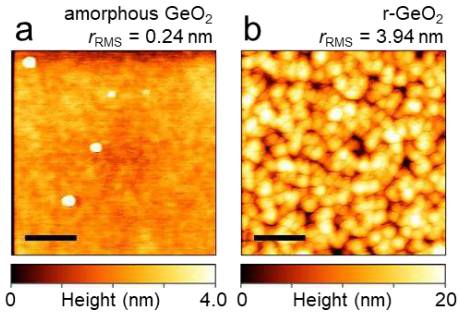

Figure 4. AFM image of (a) amorphous GeO_2 and (b) r-GeO_2 epitaxial thin film. The scale bar is 500 nm.